Biochimica et Biophysica Acta 1840 (2014) 146–152

Contents lists available at ScienceDirect

Biochimica et Biophysica Acta

journal homepage: www.elsevier.com/locate/bbagen

Dielectric characterization of costal cartilage chondrocytes

Michael W. Stacey [a], Ahmet C. Sabuncu [b,c], Ali Beskok [d,*]

[a] Frank Reidy Research Center for Bioelectrics, Old Dominion University, Norfolk, VA 23508, USA
[b] Department of Mechanical Engineering, Istanbul Technical University, Istanbul 34437, TURKEY
[c] Institute of Micro & Nanotechnology, Old Dominion University, Norfolk, VA 23508, USA
[d] Department of Mechanical Engineering, Southern Methodist University, Dallas, TX 75205, USA

ARTICLE INFO

Article history:
Received 30 March 2013
Received in revised form 24 July 2013
Accepted 29 August 2013
Available online 7 September 2013

Keywords:
Dielectric spectroscopy
Chondrocyte
Cartilage
Microfluidics

ABSTRACT

Background: Chondrocytes respond to biomechanical and bioelectrochemical stimuli by secreting appropriate extracellular matrix proteins that enable the tissue to withstand the large forces it experiences. Although biomechanical aspects of cartilage are well described, little is known of the bioelectrochemical responses. The focus of this study is to identify bioelectrical characteristics of human costal cartilage cells using dielectric spectroscopy.
Methods: Dielectric spectroscopy allows non-invasive probing of biological cells. An in house computer program is developed to extract dielectric properties of human costal cartilage cells from raw cell suspension impedance data measured by a microfluidic device. The dielectric properties of chondrocytes are compared with other cell types in order to comparatively assess the electrical nature of chondrocytes.
Results: The results suggest that electrical cell membrane characteristics of chondrocyte cells are close to cardiomyoblast cells, cells known to possess an array of active ion channels. The blocking effect of the non-specific ion channel blocker gadolinium is tested on chondrocytes with a significant reduction in both membrane capacitance and conductance.
Conclusions: We have utilized a microfluidic chamber to mimic biomechanical events through changes in bioelectrochemistry and described the dielectric properties of chondrocytes to be closer to cells derived from electrically excitably tissues.
General significance: The study describes dielectric characterization of human costal chondrocyte cells using physical tools, where results and methodology can be used to identify potential anomalies in bioelectrochemical responses that may lead to cartilage disorders.

1. Introduction

Dielectric spectroscopy is a non-invasive and label-free way to derive electrical properties of sub-cellular units. Usually a small voltage is introduced to a cell suspension that is fixed between two electrodes and resulting current is measured to obtain dielectric spectrum. Reviews by Pethig [1], Stuchly [2], Schwan and Foster [3], Pethig and Kell [4], and Foster and Schwan [5] discussed bulk dielectric properties of cells and relevant dielectric models. The effects of various stimuli can be sensed and characterized by dielectric spectroscopy. For example, the conformational changes in biological cells induced by intense pulsed electric fields were investigated by dielectric spectroscopy [6]. Dielectric measurement was also utilized to monitor the viability of cells [7]. Detection of nanoholes on erythrocyte ghosts cell membrane by dielectric spectroscopy was shown [8]. Furthermore, advancement of microfabrication technologies enabled single cell dielectric measurements, and new type flow cytometers that can work based on dielectric footprint of cells [9].

Chondrocytes are highly differentiated cells that deposit proteins that form the extracellular matrix of cartilage. Appropriate proteins are deposited as a response to biomechanical forces experienced by the cells. The bioelectrochemical milieu in which the cells reside and respond to is also of importance and is a result of the charged structure of cartilage. Chondrocytes, among other structural proteins, secrete aggrecan and associated chondroitin and keratin sulfates [10]. These molecules are highly negatively charged and create a fixed charge density (FCD) in the tissue [11]. The FCD draws Na^+ ions and water into the tissue resulting in an osmotic pressure buildup inside the tissue. The osmotic pressure is largely responsible for resisting the large forces experienced by cartilage. Cells and proteins are immobile in the tissue, whereas charged ions and water are free to move. Thus, when cartilage undergoes rhythmic compression and relaxation (e.g. during running) then water and ions move within the tissue, exposing cells to large fluxes in ionic and osmotic gradients. To maintain homoeostasis, cells need to quickly respond to these gradients, and it is apparent that to achieve this chondrocytes express an array and diversity of ion channels typically seen only in electrically excitable tissues like nerve and muscle [12]. As a result of the presence of ion channels, and therefore the ability to move large numbers of ions rapidly across the cell membrane [13],

* Corresponding author. Tel.: +1 214 768 3200; fax: +1 214 768 1473.
E-mail address: abeskok@lyle.smu.edu (A. Beskok).

0304-4165/$ – see front matter © 2013 Elsevier B.V. All rights reserved.
http://dx.doi.org/10.1016/j.bbagen.2013.08.031

we hypothesized that dielectric properties of chondrocytes would be similar to excitable versus non-excitable tissue derived cells. The use of a relatively non-specific ion channel blocker gadolinium (Gd), a blocker of cation-selective mechanosensitive channels [14], to alter dielectric properties added weight to the notion that ion channels act as a key mechanism of cellular homeostasis in chondrocytes. In this study, the dielectric spectrum of human T-cell leukemia (Jurkat), mouse melanoma (B16), rat cardiomyoblast (H9C2), and human costal chondrocyte (PC5 and PC6) cell lines is measured using microfluidic impedance spectroscopy in β dispersion regime. Jurkat and B16 cells, although metabolically active cancer cell lines, are not known to possess extensive ion channels and will act as comparative cell types to H9C2, a cell type with active ion channels and chondrocytes.

The measured impedance is modeled using a combination of physical models, such as Cole–Cole, Constant Phase Angle, Maxwell–Wagner mixture, and double shell models. Subcellular dielectric parameters, such as conductance and capacitance of the cell membrane and nuclear envelope, and conductivity of the cytoplasm and nucleoplasm, are obtained as a result of dielectric modeling. The *objective* of this study is to identify bioelectrical characteristics of costal chondrocytes using cellular dielectric properties and to our knowledge this is the first investigation of this interesting cell type.

2. Materials and methods

2.1. Microfabrication

The electrode geometries for the impedance device are obtained by standard photolithography techniques. Pre-cleaned microscope slides (Gold Seal micro slide, Gold Seal) are used as substrates for the device. First, glass slides are cleaned in 1 M KOH and acetone in an ultrasonic bath. The slides are then rinsed with DI water (Simplicity, Millipore) and desiccated on a hot plate at 120 °C for 10 min. Positive photoresist (S1805, MicroChem) is spin coated on glass slides at 4000 rpm for 30 s to achieve 0.5 μm photoresist thickness. Soft baking is applied on a hot plate at 120 °C for 1 min. The photoresist layer is exposed to 405 nm ultraviolet light (UV light source, Exoteric Instruments) for 3 s with an exposure dose of 11.74 mJ/cm^2. After keeping the wafers at room temperature for 5 min, the substrates are then developed in MF24A developer for 1 min. After rinsing the slides with DI water and subsequent baking, the slides are placed in plasma cleaner for 30 s to etch excessive photoresist. 10 nm-thick Cr and 50 nm-thick Au layers are deposited on the substrate using a metal sputtering chamber (K675XD, Emitech). The electrodes of impedance chips are fabricated by applying a lift-off process in acetone. Micro-molds are manufactured by a computer numeric control machine tool. The spacers of impedance chips are obtained by casting Sylgard 184 (PDMS) silicon elastomer in machined molds. The thickness of the spacer for impedance chip is 250 μm. The impedance chips are fabricated by aligning two electrodes on top of each other and bonding them to the PDMS spacer that is in between. In this way, a parallel plate capacitor was formed. The PDMS is functionalized by exposing it to RF plasma for 1 min at 600 mTorr and 30 W. Strong binding occurred between glass and PDMS after joining them with slight pressure under a stereoscope. The fluidic inlets and outlets of microfluidic chambers were drilled by a diamond drill bit before joining the two pieces of electrodes. The schematic and picture of the impedance chip are shown in Fig. 1.

2.2. Cell lines

Dielectric spectroscopy experiments were performed on established cell lines Jurkat (human T-cell leukemia), B16F10 (mouse melanoma), and H9C2 (rat cardiomyocytes), and on primary human costal cartilage chondrocyte cells. Chondrocytes were isolated from costal cartilage of two patients with pectus carinatum (PC) undergoing surgical repair at the Children's Hospital of the King's Daughters, Norfolk, VA, with full consent and IRB approval of Eastern Virginia Medical School and Old Dominion University. Jurkat and PC cells are grown in Roswell Park Memorial Institute Medium (RPMI; ATCC, USA) and chondrocyte growth medium (Cell Applications Inc., USA), respectively. B16 and H9C2 cells are grown in Dulbecco's Modified Eagle Medium (DMEM; Atlanta Biologicals, GA, USA). All growth media except chondrocyte growth medium are supplemented with glutamine, penicillin, streptomycin and 10% fetal bovine serum. All cells are grown in a humidified atmosphere with 5% CO_2 at 37 °C. Cells exposed to gadolinium (Gd) were incubated with 10 μM gadolinium in HB1 buffer for 1 h prior to characterization experiments. HB1 buffer, a phosphate free buffer constitutes of 136 mM NaCl, 5 mM KCl, 2 mM $MgCl_2$, 10 mM Glucose, and 10 mM HEPES (4-(2-hydroxyethyl)-1-piperazineethanesulfonic acid). All the cells are suspended in low conductivity (LC) buffer consisting of 229 mM sucrose, 16 mM glucose, 1 μM $CaCl_2$, and 5 mM NaH_2PO_4/Na_2HPO_4 in double distilled water (pH 7.4) for dielectric spectroscopy, after a washing step with isotonic buffer. The pH of LC and HB1 buffers is adjusted to 7.4 by the addition of NaOH or H_2PO_4. The electrical conductivity of the isotonic buffer is adjusted by adding phosphate buffered saline (PBS). The measurements are performed immediately after the suspension of cells in LC buffer in order to minimize the effects of the buffer. In the modeling procedures all cells are assumed as perfect spherical particles. This is a reasonable approximation as cells become nearly spherical after non-spherical adherent cells (B16F10, H9C2, and PC) were harvested from the culture flask by trypsinization. Cell size is determined by image processing the optical microscope images. Cell nucleus is marked with Hoechst fluorescent stain for sizing purposes.

2.3. Impedance measurements

A precision impedance analyzer (4294A, Agilent, Santa Clara, CA) is used for the cell impedance measurements in this study. Dielectric properties of cells are derived by modeling the measured impedance. The details of the impedance measurement technique and relevant data treatment to extract cell dielectric properties are given in a previous study [15]. In this study precision and accuracy of the device and methodology were also addressed.

In this study Maxwell–Wagner mixture, single and double shell models are utilized to find cell dielectric data, as previously used by other studies [16,17]. The following steps are taken:

1) Measured impedance is fitted into a combination of constant phase element and Cole–Cole model. In this step the effect of electrode polarization is extracted.
2) Cell suspension dielectric spectrum is fitted into Maxwell–Wagner mixture model. Clausius–Mossotti factor is obtained.
3) Cell dielectric data is fitted to double shell model. Cell dielectric parameters are obtained.

Below each of these steps is described in detail. Constant phase element is used to model electrode polarization, which is given as:

$$Z_{dl} = \frac{\kappa^{-1}}{(i\omega)^{\alpha}}, \tag{1}$$

where κ and α are constants, and ω is the angular frequency of the applied field. Cole–Cole model is used to model complex suspension permittivity ε^*_{sus}, which is given as:

$$\varepsilon^*_{sus} = \varepsilon_\infty + \frac{(\varepsilon_s - \varepsilon_\infty)}{1 + (i\omega\tau_{rel})^{\beta}} - \frac{\sigma}{\omega\varepsilon_0}, \tag{2}$$

where ε_s and ε_∞ are limiting low and high frequency values for permittivity, respectively, and σ is the static (DC) conductivity of the material. The inverse of the relaxation frequency is denoted by τ_{rel}. In the above equation β converges to 1 for single dispersion; whereas it converges to 0 for a dispersion occurring in infinite time. The fitting procedure

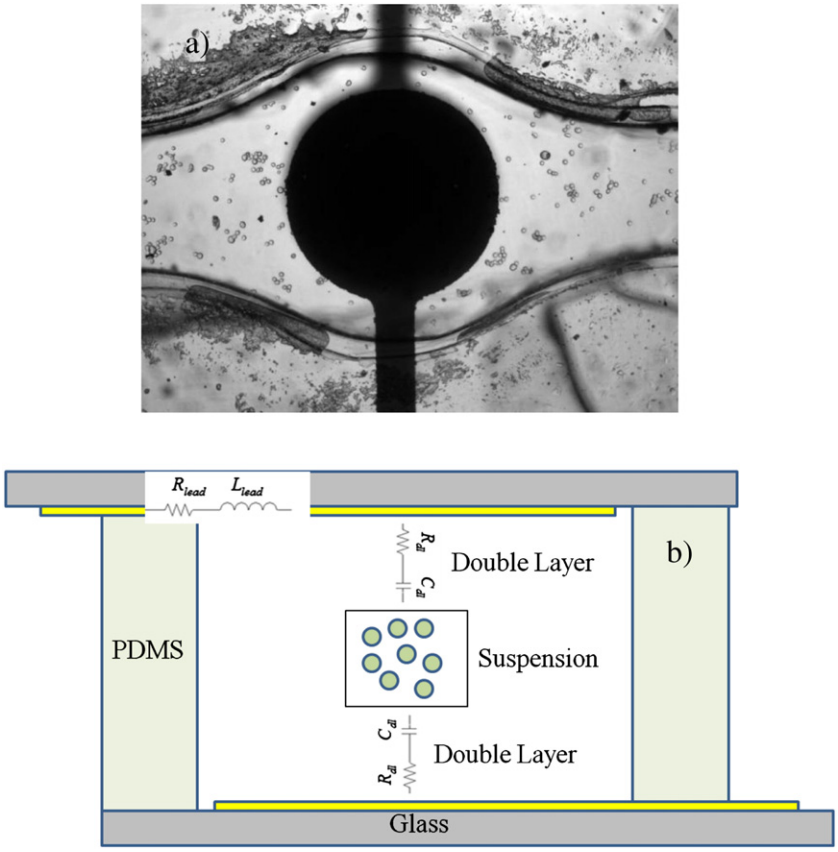

Fig. 1. Picture (a) and schematic (b) of the microfluidic device. Darker parts in the picture are electrodes. Top and bottom electrodes measure the impedance of the cell suspension in between. The schematic of the device also depicts the electrical contributions of the elements.

varied the values of the quantities in the Cole–Cole model until the difference between the model and the measurement is minimized. From the first part of the fitting, the parameters for electrode polarization (κ and α) are obtained.

The second part of the fitting uses several models to derive parameters for single cells. The electrode polarization parameters obtained from the first fitting part are used in the second part. Maxwell–Wagner mixture model is used to derive complex permittivity of a single cell from cell suspension. The model is given below:

$$\varepsilon^*_{sus} = \varepsilon^*_m \frac{1 + 2pf_{cm}(\varepsilon^*_{cell}, \varepsilon^*_{med})}{1 - pf_{cm}(\varepsilon^*_{cell}, \varepsilon^*_{med})}, \tag{3}$$

where f_{cm} (Clausius–Mossotti factor) is,

$$f_{cm} = \frac{(\varepsilon^*_{cell} - \varepsilon^*_{med})}{(\varepsilon^*_{cell} + 2\varepsilon^*_{med})}. \tag{4}$$

In the above equations *cell* and *med* are indices for cell and medium, respectively, and p is the volume fraction. In the equations * denotes complex variable. ε^* is the complex permittivity ($\varepsilon^* = \varepsilon_r - j\sigma/\varepsilon_0\ \omega$). Maxwell–Wagner model requires volume fraction of cells as an input. The volume fraction of cells is determined by centrifuging suspension in hematocrit tubes before the measurements.

Single and double shell models are used to fit the measured spectrum to derive parameters for subcellular compartments. The single shell model is given as:

$$\varepsilon^*_C = \varepsilon^*_{mem} \frac{2(1-\gamma_1)\varepsilon^*_{mem} + (1+2\gamma_1)\varepsilon^*_{cyt}}{(2+\gamma_1)\varepsilon^*_{mem} + (1-\gamma_1)\varepsilon^*_{cyt}}, \tag{6}$$

where subscripts *c*, *mem* and *cyt* are for cell, membrane, and cytoplasm, respectively. The factor γ_1 is given as, $\gamma_1 = (1 - t/a)^3$, where t is the membrane thickness, and a is the cell radius. Double shell model is given as:

$$\varepsilon^*_c = \varepsilon^*_{mem} \frac{2(1-\gamma_1) + (1+2\gamma_1)E_1}{(2+\gamma_1) + (1-\gamma_1)E_1}. \tag{7}$$

The parameter E_1 is given as:

$$E_1 = \frac{\varepsilon^*_{cyt}}{\varepsilon^*_{mem}} \frac{2(1-\gamma_2) + (1+2\gamma_2)E_2}{(2+\gamma_2) + (1-\gamma_2)E_2}, \tag{8}$$

where $\gamma_2 = (a_n/(a - t))^3$, and a_n is the radius of the nucleus. E_2 is given by:

$$E_2 = \frac{\varepsilon^*_{ne}}{\varepsilon^*_{cyt}} \frac{2(1-\gamma_3) + (1+2\gamma_3)E_3}{(2+\gamma_3) + (1-\gamma_3)E_3}, \tag{9}$$

where $\gamma_3 = (1 - t_n/a_n)^3$, $E_3 = \varepsilon^*_{np}/\varepsilon^*_{ne}$, and t_n is the nuclear envelope thickness, *np* and *ne* stands for nucleoplasm and nuclear envelope, respectively.

Estimated membrane permittivity and conductivity values using the above methodology do not reflect the true permittivity and conductivity of the membrane as double shell model does not include effects of micro-morphological features, such as protrusions, microvilli, and folds. Furthermore, membrane thickness of cells, which is a parameter in double shell model, is not measured for each cell line. Therefore, plasma and nuclear membrane properties are expressed as specific capacitance and conductance values in order to account for these geometrical effects. Membrane specific capacitance and

Table 1
Constants used in the fitting routine.

t (nm)	7
t_n (nm)	40
ε_{med}	80
ε_{cyt}	60
ε_{np}	120

resistance of the cell membrane are calculated by the following equations:

$$C_{spec} = \frac{\varepsilon\varepsilon_0}{t}$$
$$G_{mem} = \frac{\sigma_{mem}}{t}. \quad (10)$$

Cell's dielectric spectrum is obtained for frequency range 10 kHz–10 MHz. In this frequency range dielectric spectrum is mainly affected by cell size, shape, and plasma membrane [18]. Certain parameters of cells in the models, such as cytoplasm and nucleoplasm relative permittivity, are fixed in the fitting routine in order to increase the reliability of the fitting. The constants in the routine are either measurable quantities or the spectra are insensitive to their variation [17]. The constants used in the fitting routine are summarized in Table 1. The parameters that gave minimum difference between fitted and measurement data (residual) are used to characterize cells. The fitting procedures are performed in MATLAB® (2011a, Mathworks) using the nested *lsqnonlin* function that utilizes an algorithm to minimize the sum of the squares of the residuals. Also all the measurements are taken at least 3 times using different parts from suspensions.

2.4. Statistics

Statistical analysis was performed using Student t-test to determine significance between sample means of at least three independent experiments. For all tests, $p < 0.05$ indicated the difference as significant.

3. Results and discussion

Radii of cells and nuclei are determined prior to dielectric measurements and are given in Table 2. It can be deduced from the table that Jurkat cells have smallest radius and largest nucleus to cell size ratio. Cell suspensions are fed into the microfluidic device and small test voltage (0.5 V unless stated) is applied to the microfluidic chamber to measure cell suspension impedance. The data is obtained as magnitude and phase angle of impedance. A computer that is interfaced to the impedance analyzer is used to acquire raw data. An in-house computer program was developed and used to extract single cell complex permittivity spectrum using Maxwell–Wagner mixture model. The real part of single cell permittivity spectra computed from experimental impedance data for Jurkat, B16, and PC5 cell lines is plotted in Fig. 2 and shows that each cell line has a different low frequency limiting permittivity value and relaxation time that is characteristic of its dielectric parameters. A double shell model is used to model single cell permittivity spectrum and extract dielectric parameters. Magnitudes of cell membrane capacitance and conductance (Table 2) are similar for H9C2, PC5, and PC6 cells with H9C2 showing greatest membrane conductance and PC5 showing greatest membrane capacitance. The cell membrane conductance and capacitance for B16 and Jurkat cells are significantly lower than those of PC5, PC6, and H9C2 cells ($p < 0.0001$). Mean membrane conductance of B16 cells is approximately half of that observed for Jurkat cells, whereas membrane conductance of PC5, PC6, and H9C2 cells is 4–5 times higher than that for B16 cells. Cytoplasm conductivity and nuclear envelope capacitance show scatter among cell types with Jurkat cells having significantly higher nuclear envelope conductance than those of other cells ($p = 0.0007$ when compared toPC5 cells). Jurkat cells are naturally occurring suspension cells and thus the architecture of these cells influencing dielectric properties may account for these differences.

Due to the lack of published data on the dielectric properties of chondrocytes, we made a comparison of this cell type to Jurkat, B16, and H9C2 cells. H9C2 line is an electrically excitable cell line derived from cardiomyocytes and which holds vast number of ion channels [19,20]; whereas, B16 and Jurkat cells are not known to have extensive ion channels. Hence, B16 and Jurkat cells will have lower membrane conductance compared to H9C2 cells. The results in Table 2 confirm this reasoning, and it can also be deduced from the table that membrane conductance of chondrocyte cells is similar to H9C2 cells. The membrane conductance values in Table 3 confirm that ionic conduction at H9C2 cell membrane is almost 3 times higher than the average of Jurkat and B16. Assuming a membrane structure composed of a lipid-protein matrix with a thickness of 7 nm, then membrane conductivity will be on the order of 0.0143 S/m^2 [21]. However, the measured values are on the order of 10^3 S/m^2. The substantial difference between measured values and the theoretical value for the cell membrane lies in the fact that electrical conduction also occurs through the cell membrane by ion channels and around the cell by ions in the double layer or mobile charge groups at the membrane. Membrane conductivity is a measure of electric conduction through and around the cell membrane; therefore, it partly reflects the number of ion channels on the cell membrane. A slight increase in membrane conductance and capacitance is observed for B16, H9C2, PC5, and PC6 cells when test voltage is increased from 0.5 V to 1.0 V. This corresponds to electric field increase in the chamber from $2 * 10^3$ V/m to $4 * 10^3$ V/m, with 250 μm gap distances. As reference, a 10 mV change in transmembrane potential corresponds to $1.5 * 10^6$ V/m electric field change. The membrane capacitance and conductance values at these two test voltages are shown in Table 3. There is an increase in mean cell conductance (Gmem) of B16 (63%), H9C2 (8.5%), PC5 (18%), and PC6 (29%) from 0.5 V to 1.0 V. Changes in mean cell capacitance (Cmem) from 0.5 V to 1.0 V are B16 (28%), H9C2 (8.5%), PC5 (−2%), and PC6 (22%). In the frequency range used in this study, the measurements are most sensitive to membrane capacitance and conductance, whereas the measurement is least sensitive to changes in nucleoplasm conductivity [22].

The relative permittivity of the membrane can be estimated to be between 2 and 2.2 if the membrane is assumed to be composed of pure lipid matrix, and a relative permittivity of 2.8 can be assigned to hydrophobic non-polar amino acids of integral, transmembrane proteins [23]. The specific membrane capacitance can be calculated to be 0.94 μF/cm^2 if proteins are assumed to compose 40% of the plasma membrane. Cholesterol, which is also known to be present in the cell membrane, was shown to have little effect on membrane dielectric properties [24]. In addition, the presence of water in aqueous pores of the membrane

Table 2
Cellular dielectric parameters, mean cell diameter, and mean value of cell nucleus to radius ratio of all cell lines studied. Values in parenthesis are the standard deviation.

	a (μm)	a_n/a	C_{mem} (μF/cm^2)	G_{mem} (S/m^2) × 10^3	σ_{cyt} (S/m)	C_{ne} (pF/cm^2)	G_{ne} (S/m^2) × 10^3	σ_{np} (S/m)
Jurkat	5.3	0.8	1.22 (0.11)	5.42 (0.62)	0.32 (0.002)	1.57 (0.01)	37.99 (8.09)	0.63(0.005)
B16	7.5	0.57	1.85 (0.42)	2.66 (0.74)	0.18 (0.11)	1.28 (0.72)	9.16 (0.63)	0.45 (0.33)
H9C2	8.8	0.59	6.83 (0.75)	14.1 (0.86)	0.22 (0.05)	1.38 (0.13)	17.2 (8.53)	0.44 (0.1)
PC5	8.2	0.57	7.47 (1.63)	9.85 (2.53)	0.16 (0.02)	1.91 (0.72)	27.3 (4.61)	0.33 (0.06)
PC6	8.7	0.52	6.29 (0.54)	12.5 (0.82)	0.12 (0.02)	1.05 (0.47)	8.44 (3.48)	0.23 (0.06)

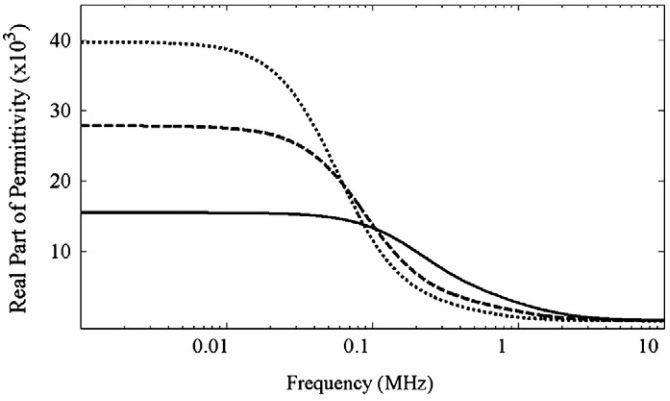

Fig. 2. The real part of single cell permittivity spectra for B16 (continuous line), H9C2 (dashed line), and PC5 (dotted) cell lines computed from experimental data using Maxwell–Wagner mixture model.

has little effect on the membrane capacitance, and therefore can be neglected [25]. Temperature dependent impedance measurements revealed that the lateral and rotational diffusions of membrane proteins are also a factor affecting the interfacial polarization [26]. Reported values of cell membrane capacitance are usually higher than 1 μF/cm^2; the difference between the theoretical value (0.94 μF/cm^2) and reported values is generally attributed to total effective surface area of a cell. The micro and nano-structures on cell membrane, such as microvilli, blebs, folds, and ruffles, were shown to affect the total cell membrane capacitance by increasing the surface area [23,27–29]. Assuming cell surface area increase as the only factor yielding higher membrane capacitances than the theoretical value, the membrane folding factor (φ_{mem}) is calculated. Membrane folding factor, which is defined as the ratio of measured membrane capacitance to the capacitance of a theoretically smooth membrane, can be used to quantify the extent of surface features [23]. Table 4 summarizes membrane folding factors for Jurkat, B16, H9C2, PC5, and PC6 cells. Membrane folding factor is calculated by dividing membrane capacitance values in Table 2 by theoretical membrane capacitance, which is 0.94 μF/cm^2. The membrane folding factor scales the same as membrane capacitance for Jurkat, B16, H9C2, PC5, and PC6 cells. According to Table 4, H9C2, PC5, and PC6 cells have around 5 times more membrane surface area than Jurkat and B16 cells, in line with the relatively higher capacitance measured in these cells. The micro and nano-structures on cell membrane increase effective cell polarizability by allowing more electrical charges to be trapped at the interface. Increased cell polarizability results in higher cell permittivity values in the low frequency. This is obvious from Fig. 2 as PC5 cells, which have the highest membrane surface area (membrane capacitance), have the highest low frequency limiting permittivity. Furthermore, it might be possible that the membrane conductance values in Table 2 do not reveal the true conductance per unit area because of the differences in total cell surface area. Therefore, the membrane conductance data in Table 2 is renormalized using the calculated membrane

Table 3
Dielectric parameters of sub-cellular units for cells at 0.5 V and 1.0 V test voltage. Values in parenthesis are standard deviation. Statistical significance is denoted by *0.5 > p > 0.1, ** 0.1 > p > 0.01, and *** p < 0.01.

	C_{mem} (μF/cm^2)	G_{mem} (S/m2) × 10^3
B16 — 0.5 V	1.85 (0.42)	2.66 (0.74)
B16 — 1 V	2.37 (0.18) **	4.34(0.25) ***
H9C2 — 0.5 V	6.83 (0.75)	14.1 (0.86)
H9C2 — 1 V	7.41 (1.05) *	15.3 (0.95) ***
PC5 — 0.5 V	7.47(1.63)	9.85 (2.53)
PC5 — 1 V	7.31 (0.82) *	11.6(1.11) **
PC6 — 0.5 V	6.29 (0.54)	12.5 (0.82)
PC6 — 1 V	7.69 (0.6) ***	16.1 (2.78) ***

Table 4
Membrane folding factor (φ_{mem}). Values in parenthesis are the standard deviation.

	Jurkat	B16	H9C2	PC5	PC6
C_{mem} (μF/cm^2)	1.22 (0.11)	1.75 (0.43)	6.83 (0.75)	7.47 (1.63)	6.29 (0.54)
φ_{mem}	1.29 (0.11)	1.86 (0.45)	7.26 (0.79)	7.94 (1.73)	6.69 (0.57)

folding factors in order to find the true capacitance per unit area. Table 5 summarizes renormalized membrane conductance values (G^*_{mem}) for Jurkat, B16, H9C2, and chondrocyte cells. Now all cell types appear to have similar mean membrane conductance values with Jurkat cells having slightly higher membrane conductance compared to other cell types. Higher membrane conductance of Jurkat cells can be attributed to the fact that Jurkat cells have less surface area than that of H9C2 cells. However, the assumptions made for calculating membrane folding factors could be open to interpretation leaving normalized membrane conductance values prone to error. Traditionally, the difference between model cell membrane capacitance and measured membrane capacitance is attributed to exterior morphological richness of cell membrane, such as the presence of microvilli, blebs, and folds on the cell membrane, while keeping the membrane thickness and permittivity constant [28,30,31]. A membrane folding factor (φ), which is the ratio of measured to model membrane capacitance, was introduced to account for the membrane's degree of morphological complexity. The proportion of saturated hydrocarbon bonds in cell membranes was recently shown to be a factor affecting specific capacitance as evidenced by Raman spectroscopy analysis [32]. A cell membrane with high proportion of unsaturated chains of hydrocarbons could have higher membrane capacitance, mainly through two reasons: 1) thinner cell membrane; and 2) relative permittivity decrease with increasing hydrogen saturation. Overall, membrane surface area, membrane thickness, and lipid content are all shown to influence specific capacitance with appropriate analysis; however, range and order of magnitude analysis of each parameter in a single characterization study are missing.

Cell membrane capacitance measurements are also available by patch clamp technique. Several previous studies obtained high membrane capacitances comparable to the values given in this study, albeit that different cell types were investigated. Kado et al. measured membrane potential, capacitance, and resistance of *Xenopus* oocytes as they undergo induced meiotic maturation [33], and reported membrane capacitance values as high as11.87 μF/cm^2. The high membrane capacitance of immature oocytes was attributed to the presence of microvilli, folds, and crypts on the membrane, increasing membrane capacitance by increasing total cell surface area. Other investigators also reported similar values for membrane capacitance on *Xenopus* oocytes [34,35].

Effects of the ion channel blocker Gadolinium (Gd) on B16, H9C2, and PC5 cells were also tested using the microfluidic device. Dielectric properties of cells measured before and after incubation are summarized in Table 6. In all cells studied there is a decrease in cell membrane conductance and capacitance. The decrease in conductance for H9C2 and PC5 cells is highly significant in Gd exposed cells compared to unexposed control ($p < 0.0001$ for each respectively). The mean membrane capacitance of all of the cells tested drops significantly, particularly in H9C2 cells, known to have extensive ion channels and chondrocytes. However, there is still statistically significant difference after Gd treatment between membrane conductance of PC5 and B16 cells ($p = 0.0047$), H9C2 and B16 cells ($p < 0.0001$), and PC5 and H9C2 cells ($p < 0.0001$) which may be a reflection of the diversity of

Table 5
Renormalized (G^*_{mem}) and original (G_{mem}) membrane conductance values. Values in parenthesis are the standard deviation. The unit of the values is (S/m^2).

	Jurkat	B16	H9C2	PC5	PC6
G_{mem}	5.42 (0.62)	2.53 (0.78)	14.1 (0.86)	9.85 (2.53)	12.5 (0.82)
G^*_{mem}	4.20 (0.48)	1.36 (0.41)	2.09 (0.91)	1.24 (0.31)	1.86 (0.12)

Table 6
Dielectric parameters of sub-cellular units for cell lines after 1 h incubation with 10 pM Gadolinium. Values in parenthesis are the standard deviation. Significance of difference between control and Gd group is denoted by *0.5 > p > 0.1, ** 0.1 > p > 0.01, and *** p < 0.01.

	C_{mem} (pF/cm^6)	G_{mem} (S/m^2) × 10^3	σ_{cyt} (S/m)	C_{ne} (pF/cm^2)	G_{ne} (S/m^2) × 10^3	σ_{np} (S/m)
B16 Control	1.75 (0.43)	2.53 (0.78)	0.15 (0.11)	1.01 (0.56)	3.76 (4.2)	0.35 (0.31)
B16 Gd	1.45 (0.4) *	1.76 (0.56) **	0.22 (0.13) *	1.51 (0.51) **	8.27 (5.49) **	0.57 (0.33) *
H9C2 Control	6.83 (0.75)	14.1 (0.86)	0.22 (0.05)	1.38 (0.13)	17.2 (8.53)	0.44 (0.1)
H9C2 Gd	2.09 (0.6) ***	5.02 (1.18) ***	0.26 (0.15) *	1.61 (0.08) *	6.51 (0.22) **	1.2 (0.43) **
PC5 Control	7.47 (1.63)	9.85 (2.53)	0.16 (0.02)	1.91 (0.72)	27.3 (4.61)	0.33 (0.06)
PC5 Gd	2.57 (0.34) ***	0.93 (0.54) ***	0.1 (0.03) ***	1.59 (0.08) *	17.5 (15.2) ***	0.26 (0.13) **

ion channels present in each cell type. There is also a significant decrease in nuclear envelope conductance of PC5 cells after Gd treatment.

Gd is known to block stretch activated channels (SAC) of chondrocyte cells [36], and also affects L-type, T-type, and N-type Ca^{2+}, Na^+, K^+, and Ca^{2+}activated Cl^- channels on other cell types [37]. The decrease in ionic transport across the membrane manifests itself in low membrane conductance values. Significant decrease in nuclear envelope conductance of PC5 cells indicates internalization of Gd, however the nucleus is a complex structure with numerous nuclear pores and membrane attachment to other subcellular structures like the endoplasmic reticulum, and therefore caution in data interpretation is warranted. Significant decreases in cell membrane capacitance values are also observed for H9C2 and PC5 cells, and although implicating changes in surface area, other mechanisms leading to this data are possible. For example, charge groups on cell membrane surface, such as proteins, lipids, and adsorbed polyelectrolytes, hold negative charge at physiological pH; therefore, cells in nature are mostly negatively charged. Surface charge attracts counter-ions from the extracellular medium, and a compact layer that is one or two ion diameter thick forms closer to cell surface, which is referred as Stern layer in colloidal science. Outside the Stern layer a larger layer, typically on the order of 10–100 nm thickness, is formed, which is referred as diffuse layer. Lateral components of membrane conductance include ionic conductance contributions at the Stern and diffuse layers. Initially the stagnant (Stern) layer might seem electrically non-conductive, as the ions are strongly bound to surface; however, experimental evidence on colloids indicates that ionic conductance occurs at the stagnant Stern layer as well [38]. Electrophoretic mobility data, which is a strong function of surface charge, on more than 300 types of cells suggest that cells of multicellular organisms scatter within ±50% of the electrophoretic mobility of red blood cells [39]. Based on this we assume that the cells investigated in this study have similar surface charge, and we can assume 0.05 C/m^{2}as cell surface charge, which is a typical value for biological cells [40]. Using a first order approximation for surface conductance ($\sigma_{sur} = \rho_{sur}\, u_{sur}$, where *sur* represents surface, u is the ion mobility, and ρ is charge) and assuming that Na^+ is the only ion type contributing to surface conduction, we obtained surface conductance values on the order of 100 S/m^2. In the above analysis ionic mobility of Na^+ at the stagnant layer is assumed to be the same as the bulk value, which is also observed in liposome vesicles [38]. This surface conductance value is similar to those given in the literature [31,41]. Accordingly, the surface conductance of cells is about 2 orders of magnitude smaller than the mean membrane conductance values in Table 2. Even though there could be variations of surface charge between cell types, these variations could not be attributed as the fundamental reason for the differences in electrophysiological characteristics because of its low contribution to overall membrane conductance. One might argue that binding of Gd cations on negatively charged groups on cell membrane could decrease the net surface charge [42], and hence the surface conduction. However, this decrease will be minute due to the following reasons. The molarity of Gd is low (10 μM) in the extracellular medium, and in order to have about 20% decrease in surface conductance at 20% cell volume fraction, all Gd ions in suspension should bind to surface groups and acquire zero mobility, which is unlikely. In addition, according to the analysis above, surface conductance constitutes only about 1 to 5% of total membrane conductance, and therefore, fluctuations in surface conductance cannot be the reason for large deviations in total membrane conductance values in Table 6. The decrease in membrane conductance after incubation with Gd is therefore likely to be associated with blocking of ion channels.

The main advantage of using a microfluidic chamber, which has a 500 μm radius and approximately 250 μm thick, is the ability to have fewer cells for measurement. Usually volume fraction values used for dielectric spectroscopy are on the order of 10%. Preparation of a corresponding number of cells is costly and not economical if a large measurement volume is chosen. The microfluidic chamber allowed us to work with fewer cells. Around 1000 cells fit inside the microfluidic chamber assuming average numbers for cell radius and volume fraction. A venue of future research is to probe low frequency dielectric dispersion of cells, which is a strong function of surface charge. This way total membrane conductance could be separated into its compartments. Another advantage of microfluidics systems, which is the focus of future work, is the ability to tune the external environment of cells. For instance the ion channel blocker Gd could have been introduced to cells that are growing in the microfluidic chamber and response to Gd could have been instantaneously sensed by dielectric spectroscopy. The use of a microfluidic approach to change the bioelectrochemical milieu and directly measure chondrocyte response is planned. Importantly, the generation of ionic and osmotic fluxes in a microfluidics chamber simulates the bioelectrochemical component of the cells that is created by biomechanical forces. Thus, experimentally biomechanics can be simulated through microfluidics. An inappropriate response of chondrocytes to the bioelectrochemical environment may illicit the production of inappropriate proteins with resulting dysplasia, and is currently an understudied field. In this work, we have used chondrocytes from individuals with chest wall deformities as a model system prior to experiments on chondrocytes from other sources to asses this hypothesis.

4. Conclusions

We have used a microfluidic chamber that can mimic biomechanical events through changes in bioelectrochemistry. Dielectric properties of chondrocytes are similar to those obtained from a cell type known to have extensive ion channels suggesting that the bioelectrochemical response of chondrocytes is of importance in maintaining cellular homeostasis.

The use of a relatively non-specific ion channel blocker (Gd) in reducing cell membrane conductance, particularly in cardiomyocytes and chondrocytes, suggests that ion channels are an important component of the bioelectrochemical response and are an active process in maintaining cellular homeostasis.

Acknowledgements

Research reported in this publication was supported by the National Institute of Arthritis and Musculoskeletal and Skin Diseases of the National Institute of Health under the award number R21AR063334. The content is solely the responsibility of the authors and does not necessarily represent the views of the NIH. We would like to acknowledge

Dr R.E. Kelly at the Children's Hospital of the King's Daughters, Norfolk, VA, USA for providing samples of cartilage from patients undergoing repair processes.

References

[1] R. Pethig, Dielectric properties of biological materials: biophysical and medical applications, IEEE Trans. Electr. Insul. (1984) 453–474.
[2] M. Stuchly, Dielectric properties of biological substances — tabulated, J. Microw. Power 15 (1980) 19–26.
[3] H. Schwan, K. Foster, RF-field interactions with biological systems: electrical properties and biophysical mechanisms, Proc. IEEE 68 (1980) 104–113.
[4] R. Pethig, D. Kell, The passive electrical properties of biological systems: their significance in physiology, biophysics and biotechnology, Phys. Med. Biol. 32 (1987) 933–970.
[5] K. Foster, H. Schwan, Dielectric properties of cells and tissues: a critical review, CRC Crit. Rev. Biomed. Eng. 17 (1989)(25?02).
[6] J. Zhuang, W. Ren, Y. Jing, J.F. Kolb, Dielectric evolution of mammalian cell membranes after exposure to pulsed electric fields, IEEE Trans. Dielectr. Electr. Insul. 19 (2012) 609–622.
[7] P. Patel, G. Markx, Dielectric measurement of cell death, Enzyme Microb. Technol. 43 (2008) 463–470.
[8] K. Asami, Dielectric spectroscopy reveals nanoholes in erythrocyte ghosts, Soft Matter 8 (2012) 3250–3257.
[9] H. Morgan, T. Sun, D. Holmes, S. Gawad, N. Green, Single cell dielectric spectroscopy, J. Phys. D Appl. Phys. 40 (2007) 61.
[10] M. Stacey, S. Neumann, A. Dooley, K. Segna, R. Kelly, D. Nuss, A. Kuhn, M. Goretsky, A. Fecteau, A. Pastor, V. Proud, Variable number of tandem repeat polymorphisms (VNTRs) in the ACAN gene associated with pectus excavatum, Clin. Genet. 78 (2010) 502–504.
[11] M.W. Lai, V.C. Mow, D.D. Sun, G.A. Ateshian, On the electrical potentials inside a charged soft hydrated biological tissue: streaming potential versus diffusion potential, J. Biomech. Eng. 122 (2000) 336–346.
[12] R. Barrett-Jolley, R. Lewis, R. Fallman, A. Mobasheri, The emerging chondrocyte channelome, Front. Physiol. 1 (Article 135) (2010), http://dx.doi.org/10.3389/phys.2010.00135.
[13] P.S. Ganesh Raj, B. Chanda, S.K. Gupta, M.K. Mathew, C. Jayaraman, Modeling of ion permeation in calcium and sodium channel selectivity filters, Proteins Struct. Funct. Genet. 38 (2000) 384–392.
[14] A. Lacampagne, F. Gannier, J. Argibay, D. Garnier, J.-Y. Le Guennec, The stretch-activated ion channel blocker gadolinium also blocks L-type calcium channels in isolated ventricular myocytes of the guinea-pig, Biochim. Biophys. Acta Biomembr. 1191 (1) (1994) 205–208.
[15] A.C. Sabuncu, J. Zhuang, J.F. Kolb, A. Beskok, Microfluidic impedance spectroscopy as a tool for quantitative biology and biotechnology, Biomicrofluidics 6 (2012) 034103.
[16] I. Ermolina, Y. Polevaya, Y. Feldman, B. Ginzburg, M. Schlesinger, Study of normal and malignant white blood cells by time domain dielectric spectroscopy, IEEE Trans. Dielectr. Electr. Insul. 8 (2001) 253–261.
[17] Y. Polevaya, I. Ermolina, M. Schlesinger, B.-Z. Ginzburg, Y. Feldman, Time domain dielectric spectroscopy study of human cells: II. Normal and malignant white blood cells, Biochim. Biophys. Acta Biomembr. 1419 (1999) 257–271.
[18] K. Asami, Characterization of biological cells by dielectric spectroscopy, J. Non-Cryst. Solids 305 (2002) 268–277.
[19] D. El-Ani, R. Zimlichman, TNFα stimulated ATP-sensitive potassium channels and attenuated deoxyglucose and Ca uptake of H9c2 cardiomyocytes, N. Y. Acad. Sci. 1010 (2003) 716–720.
[20] W. Wang, M. Watanabe, T. Nakamura, Y. Kudo, R. Ochi, Properties and expression of Ca2 + activated K + channels in H9C2 cells derived from rat ventricle, Heart Circ. Physiol. 276 (5) (1999) H1559–H1566.
[21] R. Pethig, Dielectric and Electronic Properties of Biological Materials, John Wiley & Sons, Ltd., Surrey, 1979.
[22] I. Ermolina, Y. Polevaya, Y. Feldman, Analysis of dielectric spectra of eukaryotic cells by computer modeling, Eur. Biophys. J. 29 (2000) 141–145.
[23] X.-B. Wang, Y. Huang, P. Gascoyne, F.F. Becker, R. Hoelzel, R. Pethig, Changes in friend murine erythroleukemia cell membranes during induced differentiation determined by electrorotation, Biochim. Biophys. Acta Biomembr. 1993 (1994) 330–334.
[24] R. Fettiplace, D.M. Andrews, D.A. Haydon, The thickness, composition and structure of some lipid bilayers and natural membranes, J. Membr. Biol. 5 (1971) 277–296.
[25] R. Pethig, D.B. Kell, The passive electrical properties of biological systems: their significance in physiology, biophysics and biotechnology, Phys. Med. Biol. 32 (1987) 933.
[26] L. Ferris, C. Davey, D. Kell, Evidence from its temperature dependence that the β-dielectric dispersion of cell suspensions is not due solely to the charging of a static membrane capacitance, Eur. Biophys. J. 18 (1990) 267–276.
[27] V. Sukhorukov, W. Arnold, U. Zimmermann, Hypotonically induced changes in the plasma membrane of cultured mammalian cells, J. Membr. Biol. 132 (1993) 27–40.
[28] Y. Huang, X.-B. Wang, F.F. Becker, P.R.C. Gascoyne, Membrane changes associated with the temperature-sensitive P85gag-mos-dependent transformation of rat kidney cells as determined by dielectrophoresis and electrorotation, Biochim. Biophys. Acta Biomembr. 1282 (1996) 76–84.
[29] R. Pethig, V. Bressler, C. Carswell-Crumpton, Y. Chen, L. Foster-Haje, M.E. García-Ojeda, R.S. Lee, G.M. Lock, M.S. Talary, K.M. Tate, Dielectrophoretic studies of the activation of human T lymphocytes using a newly developed cell profiling system, Electrophoresis 23 (2002) 2057–2063.
[30] J. Yang, Y. Huang, X. Wang, X.-B. Wang, F.F. Becker, P.R.C. Gascoyne, Dielectric properties of human leukocyte subpopulations determined by electrorotation as a cell separation criterion, Biophys. J. 76 (6) (1999) 3307–3314.
[31] R. Pethig, M.S. Talary, Dielectrophoretic detection of membrane morphology changes in Jurkat T-cells undergoing etoposide-induced apoptosis, IET Nanobiotechnol. 1 (2007) 2–9.
[32] M. Muratore, V. Srsen, M. Waterfall, A. Downes, R. Pethig, Biomarker-free dielectrophoretic sorting of differentiating myoblast multipotent progenitor cells and their membrane analysis by Raman spectroscopy, Biomicrofluidics 6 (2012) 034113.
[33] R.T. Kado, K. Marcher, R. Ozon, Electrical membrane properties of the *Xenopus laevis* oocyte during progesterone-induced meiotic maturation, Dev. Biol. 84 (1981) 471–476.
[34] K. Kusano, R. Miledi, J. Stinnakre, Cholinergic and catecholaminergic receptors in the Xenopus oocyte membrane, J. Physiol. 328 (1982) 143–170.
[35] C. Methfessel, V. Witzemann, T. Takahashi, M. Mishina, S. Numa, B. Sakmann, Patch clamp measurements on *Xenopus laevis* oocytes: currents through endogenous channels and implanted acetylcholine receptor and sodium channels, Pflugers Arch. 407 (1986) 577–588.
[36] M. Wright, P. Jobanputra, C. Bavington, D. Salter, G. Nuki, Effects of intermittent pressure-induced strain on the electrophysiology of cultured human chondrocytes: evidence for the presence of stretch-activated membrane ion channels, Clin. Sci. (Lond.) 90 (1996) (1979) 61.
[37] R.A. Caldwell, H.F. Clemo, C.M. Baumgarten, Using gadolinium to identify stretch-activated channels: technical considerations, Am. J. Physiol. Cell Physiol. 275 (1998) C619–C621.
[38] J. Lyklema, Surface conduction, J. Phys. Condens. Matter 13 (2001) 5027.
[39] G.G. Slivinsky, W.C. Hymer, J. Bauer, D.R. Morrison, Cellular electrophoretic mobility data: a first approach to a database, Electrophoresis 18 (1997) 1109–1119.
[40] G. Cevc, Membrane electrostatics, Biochim. Biophys. Acta 1031 (1990) 311.
[41] R. Pethig, L. Jakubek, R. Sanger, E. Heart, E. Corson, P.J.S. Smith, Electrokinetic measurements of membrane capacitance and conductance for pancreatic β-cells, IET 152 (2005) 189–193.
[42] F. Elinder, P. Arhem, Effects of gadolinium on ion channels in the myelinated axon of *Xenopus laevis*: four sites of action, Biophys. J. 67 (1994) 71–83.